Characteristics through the Melting Layer of Stratiform Clouds

RONALD E. STEWART,[1] JOHN D. MARWITZ AND JOHN C. PACE[2]

Department of Atmospheric Science, University of Wyoming, Laramie, WY 82071

RICHARD E. CARBONE[3]

National Center for Atmospheric Research, Boulder, CO 80307

(Manuscript received 3 January 1984, in final form 24 July 1984)

ABSTRACT

Thermodynamic and hydrometeor measurements from an aircraft flown through the melting layer of stratiform clouds over the California Valley are discussed and are compared with radar observations. An isothermal layer ~200 m thick existed at 0°C, and radar bright bands up to 36 dB(Z_e) were measured. The largest concentrations of ice particles occurred near −5°C and snowflakes melted by ~2°C. Aggregation, and possibly ice multiplication, contributed to the characteristics of the radar bright band.

1. Introduction

Much of the rain which reaches the earth's surface outside the tropics results from melted ice particles. Although other microphysical processes such as nucleation, condensation, as well as diffusion, aggregation and accretion growth have been studied extensively, research concerned with melting has been somewhat limited.

The relative lack of interest in melting is not surprising since the latent heat of fusion is approximately an order of magnitude less than the latent heat of vaporization. However, the melting process of snow in particular is quite unlike condensation, evaporation and freezing in that it is typically restricted to a very narrow layer just beneath the 0°C layer. The other processes typically may be distributed through a deep layer of the atmosphere.

Findeisen (1940) first reported that isothermal layers at temperatures near 0°C probably resulted from the diabatic process of melting snow. It has been shown by several authors that this cooling effect can be substantial (Wexler *et al.*, 1954: Wexler, 1954: Atlas *et al.*, 1969; and Pace, 1980). Calculations by Atlas *et al.* indicate that, under saturated conditions and in the absence of dynamical restoring forces, 1 mm of melted snow can produce a 300 m deep 0°C layer which results in a pressure perturbation of ~0.1 mb. Ten millimeters of melted snow will result in a 1 km deep isothermal layer and a 1 mb pressure perturbation.

After the development of radar during the mid-1940s, radar observers noticed that a layer of enhanced radar reflectivity near the melting layer (hereafter referred to as the bright band) was sometimes present. Attempts to explain this feature have resulted in inferences regarding the microphysical characteristics through the melting layer (Ryde, 1946; Cunningham, 1947; Marshall and Gunn, 1952; Atlas *et al.*, 1953; Mason, 1955; Lhermitte and Atlas, 1963, Du Toit, 1967; Ohtake, 1969 and 1970; Passarelli, 1978; Heymsfield, 1979; Humphries and Barge, 1979). As deduced by these investigators, it is felt that aggregation of snowflakes above and perhaps within the melting layer leads to the formation of large particles. Near 0°C, these become wet and their dielectric constant is essentially that of water. Their radar reflectivity is therefore enhanced by roughly a factor of 5. Upon melting, these particles collapse to much smaller sizes and also acquire much higher terminal velocities. Both these latter effects decrease their measured reflectivity. There is still some question as to the importance of particle breakup and aggregation within the melting region.

The research directed towards understanding melting within clouds has often not relied upon *in situ* measurements. Stratiform clouds provide a good environment for such field studies because these clouds are relatively steady state and horizontally uniform and also because precipitation forms mainly in these clouds by diffusion and aggregation so that melting occurs within a relatively thin layer. Another feature of some stratiform clouds, such as in the California Valley during the winter, is that the atmosphere is typically saturated and hence the confounding effects of evaporation are minimized.

The purposes of this article are to describe the

[1] Present affiliation: Atmospheric Environment Service, Downsview, Ontario, Canada.

[2] Present affiliation: USAF.

[3] NCAR is supported by the National Science Foundation.

thermodynamic and microphysical characteristics through the melting layer of stratiform clouds, to relate these characteristics to radar measurements, and to infer, where possible, the dominant physical processes. Measurements were made *in situ* by an instrumented aircraft and were supplemented by conventional radar observations during the operation of the Sierra Cooperative Pilot Project (SCPP) in California and in association with the Alberta Hail Studies in Alberta. Aircraft and radar data on three well-developed bright bands have been discussed by Pace (1980). Detailed results from the storm of 2 March 1978 are presented in this paper together with a summary of similar results from the other two cases.

2. Instrumentation

The primary source of data utilized in this study was the University of Wyoming King Air instrumented aircraft. State parameters include pressure, temperature and dewpoint temperature. Measurement capability on the aircraft has been described by Cooper (1978). Hydrometeor measurements include liquid water content by the Johnson-Williams (JW) probe, liquid water content computed from the Forward Scattering Spectrometer Probe (FSSP), and particle characteristics by three other optical spectrometer probes: 1D-P examining particles 300–4500 μm in size, 2D-C examining particles 25–800 μm in size and 2D-P examining particles 200–6400 μm in size. The 2D-C and 2D-P data were objectively edited to eliminate artifacts.

Radar data are also utilized in this study. These data were digitally recorded by the 5 cm wavelength NCAR CP-3 radar near Sheridan, California.

3. Case study: 2 March 1978

a. Background

On the morning of 2 March 1978, the King Air was launched into widespread prefrontal precipitation over the California Valley. Cloud top temperatures were < -20°C and rainfall rates near the Sierra foothills were $\sim$ <2.0 mm h^{-1}. Cloud characteristics encountered during the ascent through the melting layer will be examined hereinafter.

b. Radar and sounding information

The vertical radar reflectivity profile and temperatures observed at various levels are shown in Fig. 1. The computed heights are accurate to within $\sim$50 m and the reflectivity at each height is estimated to be accurate to within $\sim$2 dB(Z_e). The elevation scans were taken at 7.5° (0719 PST) and 12.5° (0919 PST). The beamwidths through the bright band were 250 and 150 m, respectively. The reflectivity of the bright band was therefore rather well resolved. However, an even better resolution of, say, 50 m may have resulted

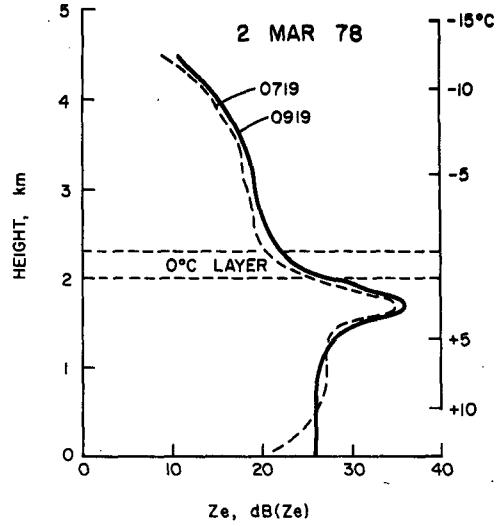

FIG. 1. Vertical profile of radar reflectivity, and the cross section of the King Air flight track from 0711 PST (takeoff) to 0725 PST on 2 March 1978. The radar data were computed from a 7.5° elevation scan of the CP-3 radar at 0719 PST and from a 12.5° elevation angle scan at 0919 PST.

in a peak dB(Z_e) value considerably greater than the observed value.

The reflectivity profiles at 0719 and 0919 LST typically agree within $\sim$1 dB(Z_e). The reflectivity profile was therefore almost constant over the 2 h period encompassing the aircraft flight. This is also consistent with the relatively steady state conditions indicated by the corresponding PPI displays. A bright band was centered at $\sim$1.8 km ($\sim$2°C) with maximum reflectivities near 35 dB(Z_e). Reflectivity at the level of the bright band was $\sim$17 dB greater than at 3 km (-5°C) and $\sim$8 to 10 dB greater than at levels below 1.3 km (+5°C). The bright band was $\sim$300 m below the base of the 0°C isothermal layer. Using the Marshall-Palmer Z–R relation, the reflectivity below +5°C corresponds to a mean rainfall of 1.7 mm h^{-1}. Surface measured rainfall rates were $\sim$1.5–2.0 mm h^{-1}.

The sounding obtained during the ascent from McClellan AFB is shown in Fig. 2. A nearly isothermal layer was present between 785 and 765 mb ($\sim$210 m) at a temperature very close to 0°C. The atmosphere, as measured, was essentially saturated from the surface to at least 575 mb except for a thin layer near 675 mb.

The equivalent potential temperature (θ_e) profile exhibits several features. Its minimum value (306 K) occurred near the base of the 0°C isothermal layer, and there was a 6 K depression from the value of θ_e at the +10°C level to the minimum alue. Furthermore, moist adiabatic ascent with roots below the isothermal layer would be predicted to each temperatures colder than -5°C, and the maximum buoyancy would be at the base of the isothermal layer. Some

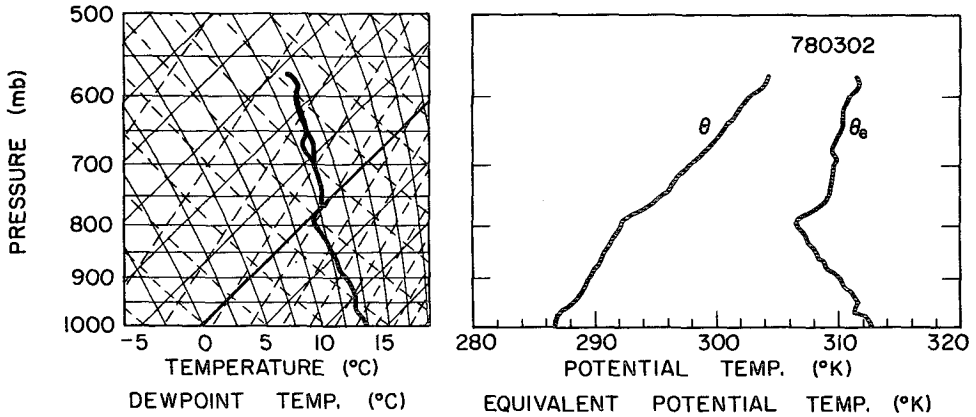

FIG. 2. The sounding obtained by the King Air between 0711 PST (takeoff) and 0754 PST on 2 March 1978.

embedded convection was encountered within the stratiform cloud region by the aircraft, but its extent was a small portion of the area.

Scatter diagram of JW and FSSP cloud liquid water contents are shown in Fig. 3. Both probes show the largest values (0.05 to 0.3 g m^{-3}) at elevations slightly below the 0°C layer. This observation was probably a direct consequence of melting crystals as well as condensation of water vapor in this chilled region.

c. *2-D images through the melting layer*

Images obtained with the 2D-C and 2D-P probes at various levels are presented in Fig. 4. These examples of the available images were chosen to illustrate significant features.

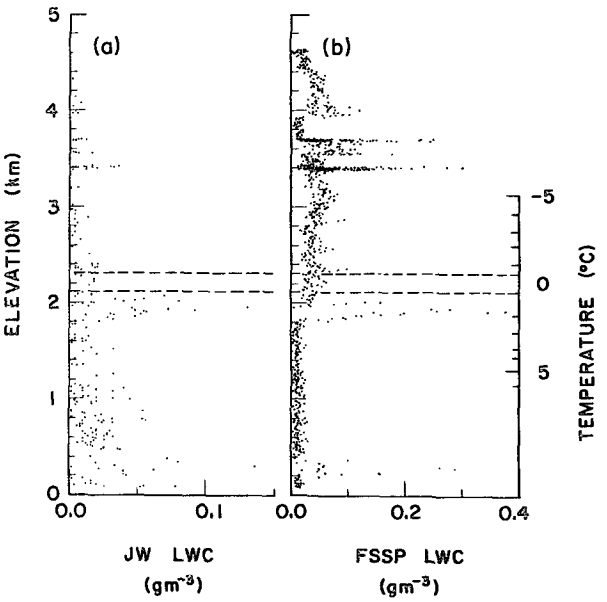

FIG. 3. Scatter diagrams of 1 s values of cloud liquid water content recorded during takeoff ascent on 2 March 1978, plotted as a function of elevation and temperature. Liquid water was measured by both the Johnson-Williams (JW) probe and the Forward-Scattering Spectrometer Probe (FSSP). The dashed lines show the extent of the 0°C isothermal layer.

There was an evolution in particle characteristics at the supercooled temperatures. At −15°C there are aggregates of dendrites as well as capped columns and bullet rosettes present in the 2D-C images. At −10°C the most common crystal habit is dendritic and several aggregates of dendrites of 5 to 6 mm sizes are apparent in the 2D-P images. At −7°C the most common crystal habit is needles but other crystal habits are also present. There were *no* graupel particles observed. At 0°C the most common images are the large aggregates.

Many of the images recorded near 0°C had rounded edges implying that melting had commenced. The large aggregates observed at this temperature were similar in shape and size to those detected at higher levels. The largest particle detected during the entire ascent (>11 mm across) was encountered near 0°C.

Images from near the 0.5°C level include the coldest circular image discernible (~600 μm diameter). Such a circular image may be due to either a partially or completely melted ice particle. It is unlikely that this particle had retained the low density characteristic of aggregates because a circular shell of water only forms at the advanced stage of melting (Knight, 1979). Except for this image, the shapes of the images changed little from ~0 to 0.5°C, although the edges of many of the larger particles appeared rounded at the warmer temperature.

The particles detected near 1.3°C were mostly circular although a few large non-circular particles (1.5–3.5 mm across) were also present. The warmest non-circular image was recorded at +2.0°C and it was >1.5 mm across.

Figure 5 is a plot of the ratio of the number of 2D-C circular images to the total number of 2D-C images as a function of temperature and the distance below the base of the 0°C layer. Only 2D-C images larger than 200 μm were considered in order to avoid

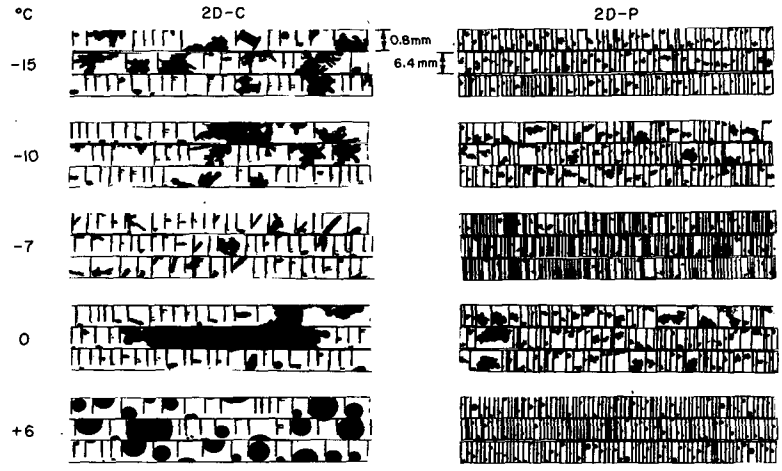

FIG. 4. 2-D images recorded during the takeoff ascent on 2 March 1978 as a function of temperature.

problems caused by probe resolution. A simple linear relation between the ratio and distance accounts for much of the data.

d. Particle size and concentration

The sizes of the largest particles observed by the 2D probes are shown in Fig. 6 as a function of height and temperature. The solid and dashed lines have been drawn to emphasize the most important features. Due to the limited sample volume of the probes, it is probable that the largest particles were not encountered. Based on the rate of climb and the sample size, the 2D-C and 2D-P probes sampled ~50 L and ~2 m^3 per 100 m of altitude, respectively. This problem is most acute for very large ice particles, which have low concentrations and for water drops which also have low concentrations. Consequently, this figure at best illustrates only general trends. The solid curve, for example, was drawn to provide an estimate of size at the 'minimum' detectable concentration of ~1 m^{-3}.

The maximum sizes of observed particles changed little between 3.3 and 2.6 km (−6 to −2°C) and increased slowly between 2.6 and 2.3 km (−2.5 to

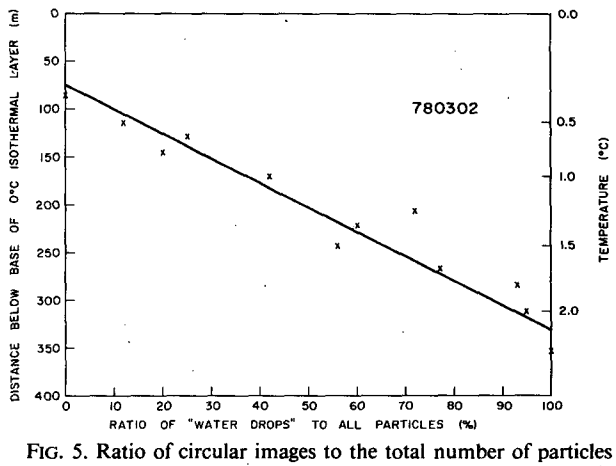

FIG. 5. Ratio of circular images to the total number of particles in each pair of 2D-C image strips recorded while the King Air ascended through the melting layer on 2 March 1978, plotted as functions of temperature and distance below the base of the 0°C isothermal layer. The solid line indicates a linear relation between ratio and distance.

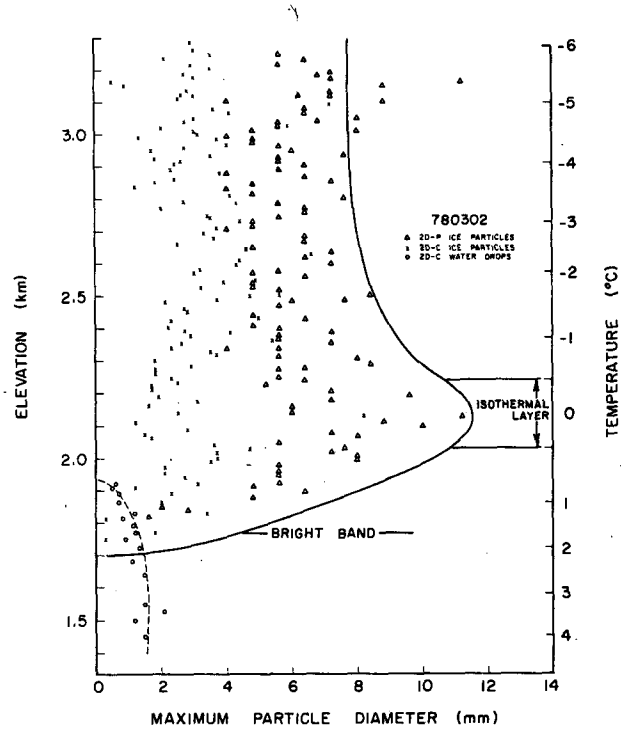

FIG. 6. Diameters of the largest particles in each pair of 2D-C and 2D-P image strips from the takeoff ascent on 2 March 1978, plotted as functions of elevation and temperature. The solid and dashed lines outline the largest particles of ice and circular images, respectively.

−1.0°C). A rapid increase in size occurred between 2.3 and 2.1 km (within the 0°C isothermal layer) and a rapid decrease occurred between 2.1 and 1.7 km (0 to 2°C). Interestingly, the temperature at the bright band level was ~2°C where particles having a concentration of 1 m^{-3} were estimated to have a diameter of only ~4 mm, although larger particles in concentration of <1 m^{-3}, were probably present as well. Another explanation is that the small sizes are a consequence of the uncertainty in the aircraft and bright band heights. A relative increase in the bright band height of 100 m (which is within the possible errors) would imply a maximum particle size of ~8 mm for particles having a concentration of 1 m^{-3}.

The largest observed circular images showed a general trend of increasing size between 1.9 and 1.7 km (0.7 to 2.0°C). This may have occurred because the largest non-circular images would likely be the last to melt.

Figure 7 shows the concentrations of particles measured by the 2D probes as functions of altitude and temperature. Both curves show peak concentrations at ~ −5°C. There was a steady and gradual decrease in concentration from near the −5°C level to the base of the 0°C level, a rapid decrease from there to about the 1°C level, and relatively invariant concentrations below. The 1D-P and 2D-C concentrations decreased by factors of ~4 and 10, respectively, from the base of the 0°C layer to the 3°C level. The peak ice crystal concentration near the −5°C level is indicative of some ice multiplication process, whereas the decrease in concentration from −5 to 0°C is indicative of aggregation.

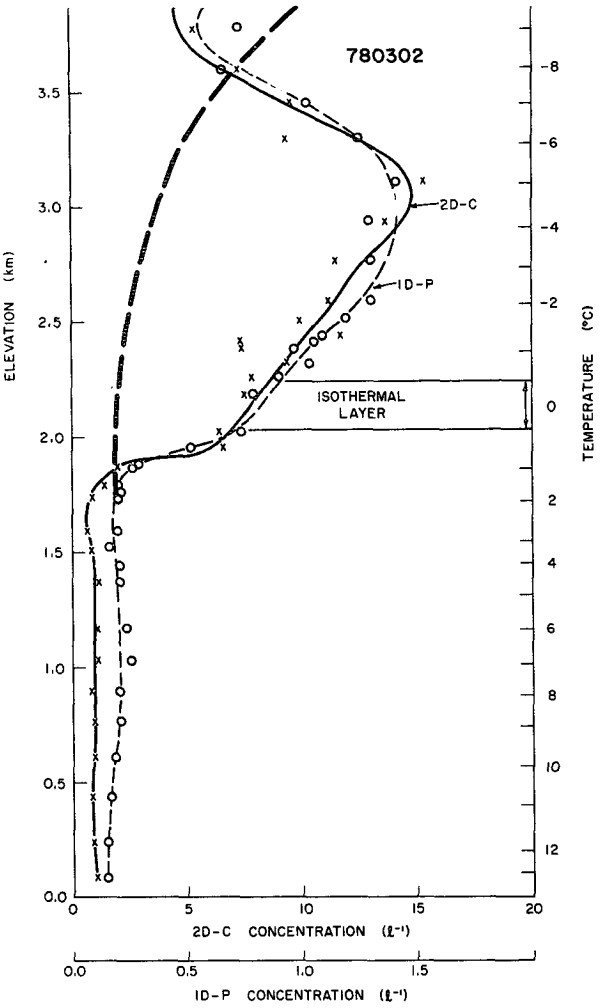

FIG. 7. Concentrations of particles detected by the 1D-P and 2D-P probes during the King Air takeoff ascent on 2 March 1978, plotted as functions of elevation and temperature.

e. Particle size distribution

Flight segments through horizontally homogeneous reflectivity regions were identified and exponential distributions (Eq. 1) were fitted by a least squares method to the measurements from the optical array probes.

$$N(D) = N_0 e^{-\lambda D} \tag{1}$$

where $N(D)$ is the number density, D is diameter which here is the largest distance across a crystal, λ is the slope parameter and N_0 is the intercept parameter.

Some representative distributions from the 1D-P, 2D-C and 2D-P probes are presented in Fig. 8. The bin value concentrations for each probe are plotted for the mean flight temperatures of +6.5, −1.0, −6.7 and −14.5°C. In accordance with Gordon and Marwitz (1984) the distributions were fitted for diameters between 1 and 4 mm and were restricted to those bins in which at least 10 hydrometeors were sampled. For diameters < 1.5 mm a hand fitted curve was drawn through the points from each probe where the distribution curves appear to depart significantly from the exponential curves.

At temperatures warmer than +3°C (below the melting level) the data from the three probes are in good agreement and they indicate that the exponential distribution is an appropriate assumption (see Fig. 8a). The slope of the curves through the 1D-P data (1 to 4 mm) was somewhat greater than the slopes through the other data. Since the sample volume of the 1D-P probe decreases substantially for the larger hydrometeors and the measured slopes differ from the 2D probes, we have restricted our use of spectral parameters to those derived from 2D probes. The fact that the three probes are in substantial agreement in rain suggests that calibrations were performed in a consistent manner and that the software treated the recorded data properly.

At T = −1.0, −6.7 and −14.5°C the three probes were in close agreement for hydrometeor diameters

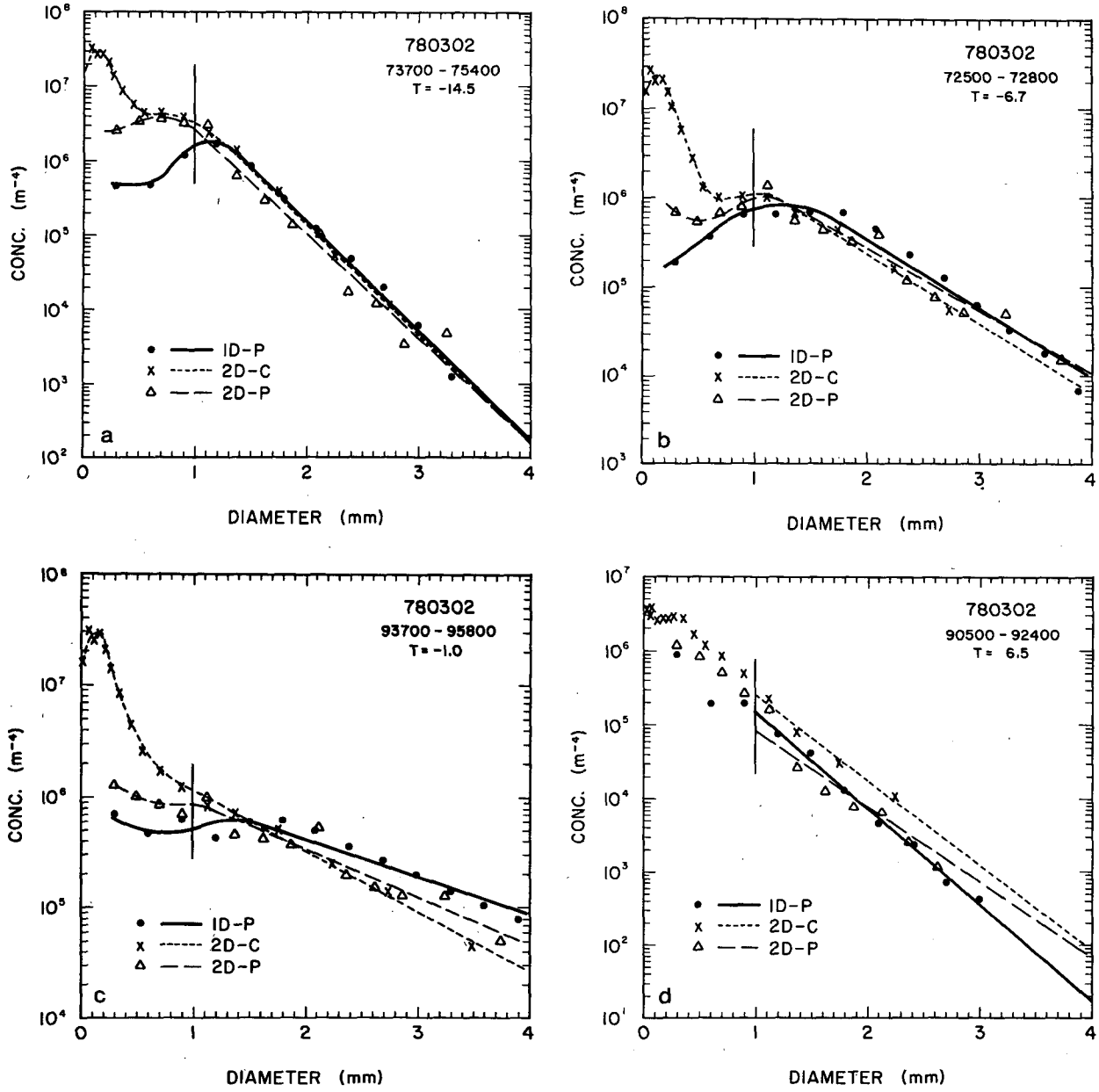

FIG. 8. The bin value concentrations for each optical array probe are plotted for the mean flight temperatures of (a) −14.5°C, (b) −6.7°C, (c) −1.0°C and (d) 6.5°C. The experimental distributions are fitted by least square method for diameters between 1–4 mm. A plotted point represents at least 10 hydrometeors. For $D < 1.5$ mm the curves through the points were drawn by hand.

between 1 and 4 mm and the bin value concentrations seem to indicate that an exponential distribution was appropriate. At $T = -1.0$°C the slopes of the fitted curves are quite flat ($\lambda \sim 1$ mm^{-1}). For diameters < 1.5 mm the 1D-P probe always recorded a subexponential distribution, the 2D-P probe recorded only a slightly subexponential distribution and the 2D-C probe almost always recorded a highly subexponential distribution. The distributions for diameters < 1.5 mm are equally complex at $T = -6.7$ and −14.5°C. The 2D-C recorded the highest concentrations while the 1D-P recorded the lowest concentrations. All of the distributions are subexponential for $D < 1$ mm except for the 2D-C distributions in the smaller categories. As pointed out by Gordon and Marwitz (1984), the probes are triggered by the narrowest dimension of a hydrometeor but the longitudinal dimension is recorded as "diameter" for the 2D probes. In the case of columns and needles with their large aspect ratios, the 1D-P has the hardest time responding and the 2D-C concentrations exceed the 1D-P concentrations by 1 to 2 orders of magnitude.

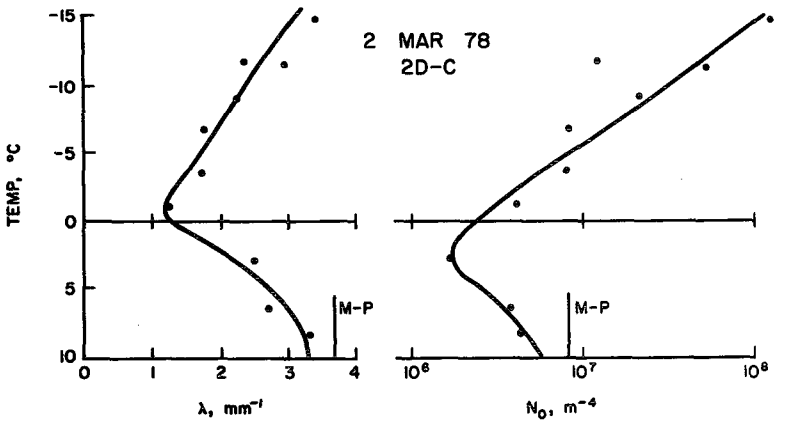

FIG. 9. Plots of slope parameter λ and intercept parameter N_0 versus mean flight temperature for several exponential distributions obtained on 2 March 1978 using the 2D-C probe. The curves were hand-fitted to the points. The Marshall–Palmer intercept and slope values for a rainfall rate of 1.7 mm h^{-1} are also indicated.

The 2D-C probe data suggest that at least some stratiform clouds in California which display a substantial bright band have a superexponential ice crystal distribution, i.e., an excess of submillimeter ice crystals exists in the temperature range from 0 to −15°C.

The slope parameter and the intercept parameter were calculated for each homogeneous flight segment. The values of λ and N_0 versus mean temperature of observation are plotted in Figs. 9 and 10 for both the 2D-C and 2D-P probes. The curves were subjectively drawn through the data points. The curves through the points for each probe were remarkably similar in shape but the values of λ and N_0 were slightly greater for the 2D-C distributions. Both λ and N_0 were inversely related to temperature above the 0°C level. These results are similar to those of Passarelli (1978), Houze *et al.* (1979) and Lo and Passarelli (1982). The minimum value of slope (1 mm^{-1}) was essentially the same as that proposed by Lo and Passarelli as being indicative of an equilibrium between aggregation and particle breakup. The fact that this value occurred close to 0°C in the present study implies that melting also limited the slope from decreasing further. Within the rain below the melting layer, the Marshall and Palmer (1948) intercept value (8×10^6 m^{-4}) exceeds the N_0 values but the limited data suggest that the distributions are evolving toward it. The slope parameter is also evolving to the M–P slope parameter for a rainfall rate of ~1.5–2.0 mm h^{-1}.

The exponential distributions for the curves of λ and N_0 of Fig. 10 (2D-P) are presented in Fig. 11 for specific temperatures. Above the 0°C level the concentrations of particles < 1.5 mm diameter varies inversely with temperature while the concentration of particles > 2.5 mm diameter varies directly with temperature. This variation of λ and N_0 is consistent with the conclusion of Lo and Passarelli (1982) that the variation in spectra in the 0°C to −15°C level implies a balance between diffusional growth and aggregation. From 0°C to +2.5°C the slope decreases

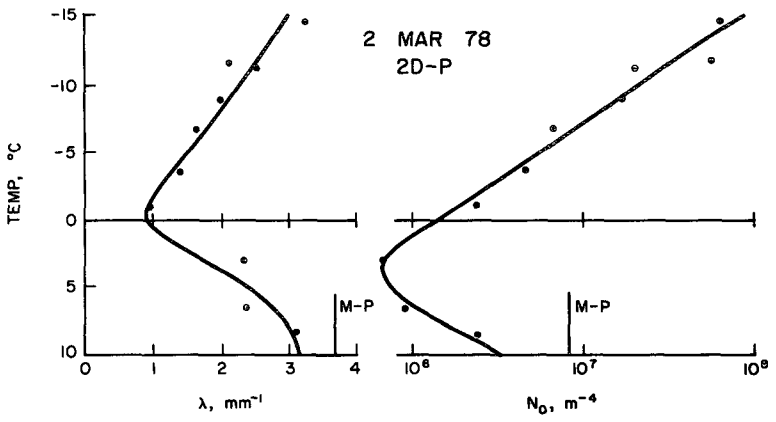

FIG. 10. As in Fig. 9 except for using the 2D-P probe.

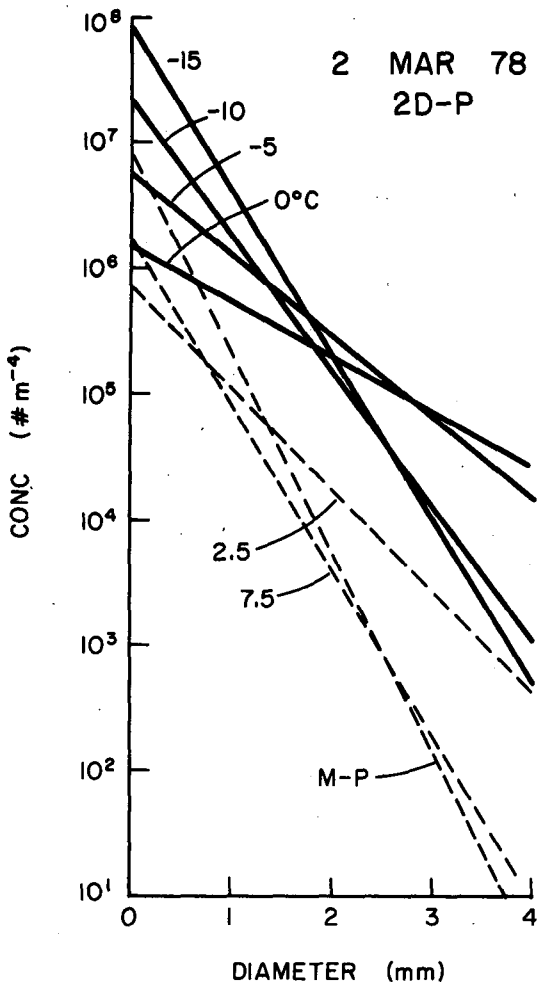

FIG. 11. Exponential distributions for the curves of Fig. 9 (2D-P) for specific temperatures. Distributions for temperatures < ~0°C are solid lines while those for temperatures >0°C are dashed lines.

and the distributions evolve slowly toward the M-P distribution for a rainfall rate of 1.7 mm h^{-1}. The distribution would be expected to evolve faster if the rainfall rate was greater, since the evolution depends upon coalescence and collisional breakup.

4. Inferred precipitation processes

a. Background

The three case studies with well-defined bright bands were synthesized in detail and the results are summarized in Table 1. The characteristics of these were quite similar except that the Alberta case was characterized by a higher rainfall rate and correspondingly higher reflectivity values. Reflectivity differences below the bright band level and melting layer depths were nevertheless almost independent of day. As discussed in the Introductory section, various suggestions have been made as to which precipitation processes are occurring near the melting layer to produce such effects. Using the present *in situ* and radar information for the 2 March 1978 case, the occurrence of various processes will now be examined.

b. Aggregation

The observations clearly show that aggregation was occurring above and throughout most of the depth of the 0°C layer. Evidence supporting this includes the 2D images, increasing particle size with increasing temperature, and a decrease in particle concentration over this temperature range.

c. Ice particle breakup near bright band level

The radar and *in situ* observations can largely be explained without considering appreciable ice particle breakup within the melting layer. The 8 dB decrease in value of reflectivity from its maximum value to that at +5°C can largely be explained by a 4 dB drop caused by fall speed changes (from ~2 to ~5 m s^{-1} below the bright band level) and by a ~3 dB shape effect resulting from non-spherical (enhanced backscatter) to spherical particles (Atlas *et al.*, 1953). The *in situ* observations also suggest that a significant contributing factor to the decrease in radar reflectivity below the melting zone is the *raindrop breakup process* which is decreasing the concentration of large drops (to be described in Section 4e). It should be noted, however, that the data used for assessing ice particle breakup are limited; furthermore, detailed observations are required to confirm these suggestions.

d. Ice multiplication

The peak in the ice particle concentration near −5°C and the presence of columnar-like crystals near this temperature are both consistent with ice multiplication occurring within the clouds. The rime splintering process proposed by Hallett and Mosop (1974) may be responsible for the observations since the observed temperature region agrees with that proposed. The observed small droplet sizes would, however, imply that this proposed process would occur more slowly than within a convective cloud existing within a maritime air mass. Other processes involving crystal breakup (such as described by Hobbs *et al.*, 1973 and Vardiman, 1978) could also contribute to the observations.

e. Raindrop spectral evolution

The spectral changes below the melting layer indicate that the raindrop size spectrum was still evolving. As indicated in Fig. 11, there was a relative decrease in the concentration of large drops and a relative increase in the concentration of small ones as the temperature increased. This is consistent with collision-induced breakup. The observation that even

TABLE 1. Summary of bright band case studies.

	2 Mar 78	6 Feb 78	16 Aug 78
Reflectivity profiles			
Z_{mx}, dB(Z_e)	35	36	47
Temp at Z_{mx}, °C	+2	+2	+2
$Z_{mx\text{-}Z}$ at −5°C, dB	17	15	27
$Z_{mx\text{-}Z}$ at +5°C, dB	8	7	7
Height of bright band below 0°C level, m	~250	300	260
Sounding			
Depth of 0°C isothermal layer, m	210	170	200
θ_e at +10°C-θ_e at 0°C base, °K	6	5	7
Hydrometeors			
Temperature first melted particle observed, °C	+0.4	+0.5	0.0
Temperature last non-spherical particle obsr., °C	+2.0	+3.5	2.5
Temperature largest particles observed, °C	0.0	+1.0	N/A
Size of largest observed particle, mm	11	16	N/A
Size of 1 m^{-3} concentration of particles at bright band level, mm	4	10	N/A
Temperature of peak particle conc., °C	−5	−7	−6
Rainfall rate, mm h^{-1}	1.7	2.0	6.5
Significant aggregation observed	yes	yes	yes
Size of largest particle at −5°C level, mm	8	7	N/A
Size of largest particle at +5°C level, mm	1.5	1.5	N/A

the ground-level size spectrum had not reached a Marshall–Palmer distribution (Figs. 9 and 10) is at least partially attributable to the relative scarcity of collisions within these low rainfall situations as pointed out by others such as Carbone and Nelson (1978). In other words, the raindrop size spectrum observed ~2 km below the melting layer was still influenced by the manner in which the melting process occurred.

5. Synthesis of observations

a. Atmospheric profiles

A schematic sounding is shown in Fig. 12 for the prefrontal cases which were examined. There is a ~200 m thick isothermal layer with the consequent increase in θ_e between the bottom and top of this layer, and a decrease in θ_e with increasing altitude below the isothermal layer. The diabatic process of melting can account for these major profile features. Since diabatic cooling produces a conditionally unstable layer, it follows that this region is subject to secondary dynamic responses such as turbulence or shallow embedded convection.

A more complete schematic diagram of many of the important thermodynamic, microphysical, and radar characteristics through the melting layer is illustrated in Fig. 13. Several important features are illustrated in this diagram. The peak in radar reflectivity occurs near 2°C or −0.3 km (all distances in the figure are relative to the base of the 0°C layer). The 2D-C concentrations (and 1D-P as well) peak

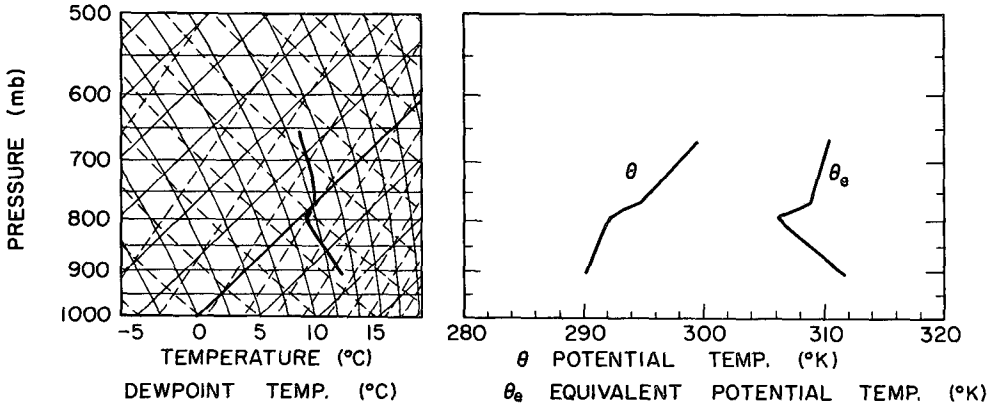

FIG. 12. Schematic sounding through typical well-developed melting layer.

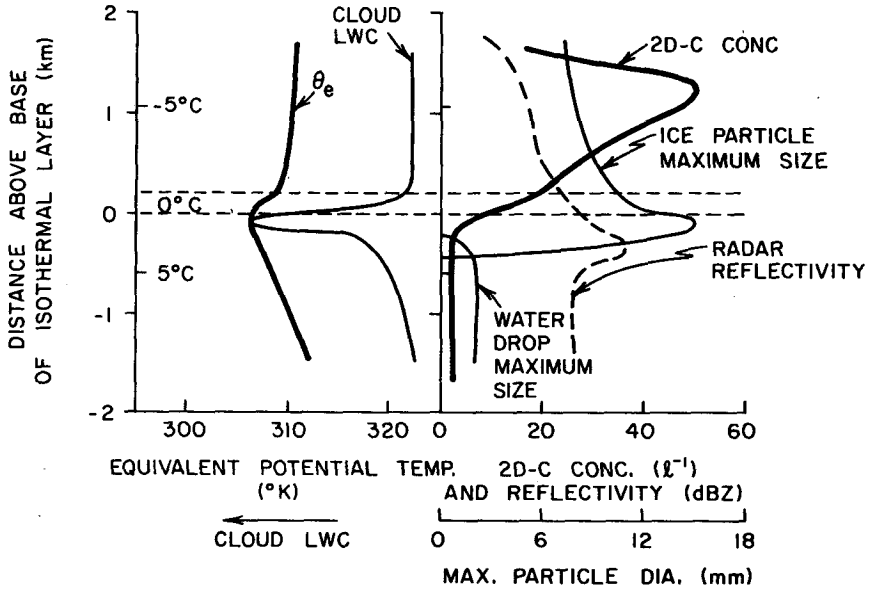

FIG. 13. Schematic profile illustrating significant trends of various microphysical and state parameters through a typical melting layer as deduced by synthesizing the observations of all the case studies.

near −5°C and thereafter decrease almost linearly with decreasing distance until ~ −0.2 km (~2°C). After this point, concentrations remain relatively constant. The maximum water drop size has been reached by ~ 0.4 km (~3°C) and thereafter is relatively constant. The cloud liquid water content reaches its largest values just below the base of the isothermal layer.

b. Precipitation processes and the bright band

This study has illustrated that aggregation occurred above, and throughout most of the depth of, the 0°C layer. This apparently results in the production of a few relatively large particles (> ~4 mm diameter on 2 March and > ~10 mm diameter on 6 February) before melting is complete. These particles, in conjunction with the smaller raindrops present at the bright band level, behave (to a first approximation) as Rayleigh scatterers to yield the maximum radar reflectivity. Significantly larger particles occur near the base of the 0°C layer. Presumably because the largest particles have an effective dielectric constant much closer to ice than water (and secondly because back scatter cross sections of highly irregular shaped particles are not well understood), the measured reflectivities appear greatest below the region where these largest particles exist.

The isothermal layer near 0°C may indirectly enhance aggregation and subsequently the bright band. As discussed by Rogers (1974) and Hobbs (1974), aggregation efficiency is directly related to temperature until melting occurs. The rapid aggregation evidenced in the isothermal layer may result because melting proceeds slowly at temperatures very close to 0°C and this is also the region of large aggregation efficiencies.

Bright band intensity is highly dependent upon the characteristics of the largest particles. In addition to aggregation, the ice particle multiplication suspected near −5°C may also play a role in forming the bright band. Columnar-like crystals formed in this manner by diffusion before aggregating themselves or, perhaps more likely before being collected by existing dendritic aggregates, tend to form large, lacy aggregates. These large aggregates would presumably be the particles which would continue to grow the fastest through aggregation and to consequently result in some of the largest semi-melted particles.

6. Summary and implications

The melting layer is an extremely complex part of a stratiform cloud. Thermodynamic and microphysical characteristics found within this region were documented. These data were used to illustrate that aggregation, ice crystal multiplication, and raindrop breakup are operating within or near the melting layer, and that the characteristics of the radar bright band are critically dependent upon such processes. These findings are reasonably consistent with the general findings of several previous investigations (Battan, 1973). Several processes occurring in this region have been verified by *in situ* hydrometeor measurements that heretofore were inferred from reflectivity and Doppler radar signatures.

Acknowledgments. This research was sponsored by the Department of Interior's Bureau of Reclamation under Contract No. 7-07-83-V0001. The contributions of all SCPP participants are sincerely appreciated.

REFERENCES

Aden, A., and M. Kerker, 1951: Scattering of electromagnetic waves by two concentric spheres. *J. Appl. Phys.*, **22**, 1242–1246.

Atlas, D., M. Kerker and W. Hitschfeld, 1953: Scattering and attenuation by non-spherical atmospheric particles. *J. Atmos. and Terr. Ph.*

——, R. Tatehira, R. C. Srivastava, W. Marker and R. E. Carbone, 1969: Precipitation-induced mesoscale wind perturbations in the melting layer. *Quart. J. Roy. Meteor. Soc.*, **95**, 544–560.

Battan, L. J., 1973: *Radar Observations of the Atmosphere.* University of Chicago Press, Chicago, IL, 324 pp.

——, and C. F. Bohren, 1982: Radar backscattering by melting snowflakes. *J. Appl. Meteor.*, **21**, 1937–1938.

Carbone, R. E., and L. D. Nelson, 1978: The evolution of raindrop spectra in warm-based convective storms as observed and numerically modeled. *J. Atmos. Sci.*, **35**, 2302–2314.

Cooper, W. A., 1978: Cloud physics investigations by the University of Wyoming in HIPLEX 1977. Department of Atmospheric Science, University of Wyoming, Laramie, 320 pp.

Cunningham, R. M., 1947: A different explanation of the "bright line". *J. Meteor.*, **4**, 163.

Du Toit, P. S., 1967: Doppler radar observation of drop sizes in continuous rain. *J. Appl. Meteor.*, **6**, 1082–1087.

Findeisen, W., 1940: The formation of the 0°C-isothermal layer and fractocumulus under nimbostratus. *Met. Zeit.*, **57**, 49–54.

Gordon, G., and J. D. Marwitz, 1984: An airborne comparison of three PMS probes. *J. Atmos. Ocean. Technol.*, **1**, 22–27.

Gunn, K. L. S., and T. W. R. East, 1954: The microwave properties of precipitation particles. *Quart. J. Roy. Meteor. Soc.*, **80**, 522–545.

Hallett, J., and S. C. Mossop, 1974: Production of secondary ice particles during the riming process. *Nature*, **249**, 26–28.

Heymsfield, G. M., 1979: Doppler radar study of a warm frontal region. *J. Atmos. Sci.*, **36**, 2093–2107.

Hobbs, P. V., 1974: *Ice Physics.* Oxford University Press, 837 pp.

——, R. J. Farber and R. G. Joppa, 1973: Collection of ice particles from aircraft using decelerators. *J. Appl. Meteor.*, **12**, 522–528.

Houze, R., P. V. Hobbs, P. Herzegh and D. Parsons, 1979: Size distributions of precipitation particles in frontal clouds. *J. Atmos. Sci.*, **36**, 151–162.

Humphries, R. G., and B. L. Barge, 1979: Polarization and dualwavelength radar observations of the bright band. *IEEE Trans. Geosci. Elect.*, **GE-174**(4), 190–195.

Knight, C., 1979: Observations of the morphology of melting snow. *J. Atmos. Sci.*, **36**, 1123–1130.

Lhermitte, R., and D. Atlas, 1963: Doppler fall speed and particle growth in stratiform precipitation. *Proc. 10th Wea. Rad. Conf.*, Boston, Amer. Meteor. Soc., 297–302.

Lo, K. K., and R. E. Passarelli, Jr., 1982: The growth of snow in winter storms: An airborne observational study. *J. Atmos. Sci.*, **39**, 697–706.

Marshall, J. S., and W. Mck. Palmer, 1948: The distribution of raindrops with size. *J. Meteor.*, **5**, 165–166.

——, and K. L. S. Gunn, 1952: Measurement of snow parameters by radar. *J. Meteor.*, **9**, 332–327.

Mason, B. J., 1955: Radar evidence for aggregation and orientation of melting snowflakes. *Quart. J. Roy. Meteor. Soc.*, **81**, 262–264.

Ohtake, R., 1969: Observations of size distributions of hydrometeors through the melting layer. *J. Atmos. Sci.*, **26**, 545–557.

——, 1970: Factors affecting the size distribution of raindrops and snowflakes. *J. Atmos. Sci.*, **27**, 804–813.

Pace, J., 1980: Microphysical and thermodynamic characteristics through the melting layer. M.S. thesis, Dept. of Atmos. Sci., AS 126, University of Wyoming, Laramie, WY, 204 pp.

Passarelli, R. E., Jr., 1978: An approximate analytical model of the vapor deposition and aggregation growth of snowflakes. *J. Atmos. Sci.*, **35**, 118–124.

Rogers, D. C., 1974: The aggregation of natural ice crystals. M.S. thesis, Dept. of Atmos. Sci., University of Wyoming, Laramie, WY, 91 pp.

Ryde, J. W., 1946: The attenuation and radar echoes produced at centimetre wavelengths by various meteorological phenomena. *Meteorological Factors in Radio-Wave Propagation,* London, The Physical Society, 169–188.

Vardiman, L., 1978: The generation of secondary ice particles in clouds by crystal–crystal collision. *J. Atmos. Sci.*, **35**, 2168–2180.

Wexler, R., 1954: Precipitation growth in stratiform clouds. *Quart. J. Roy. Meteor. Soc.*, **72**, 363–371.

——, R. Reed and J. Honing, 1954: Atmospheric cooling by melting snow. *Bull. Amer. Meteor. Soc.*, **35**, 48–51.